Inorganic Chemistry

Article

pubs.acs.org/IC

Second Sphere Control of Redox Catalysis: Selective Reduction of O_2 to O_2^- or H_2O by an Iron Porphyrin Catalyst

Subhra Samanta,[†] Kaustuv Mittra,[†] Kushal Sengupta, Sudipta Chatterjee, and Abhishek Dey*

Department of Inorganic Chemistry, Indian Association for the Cultivation of Science, Jadavpur, Kolkata 700032, India

Supporting Information

ABSTRACT: "Click" reaction has been utilized to synthesize porphyrin ligands possessing distal superstructures functionalized with ferrocenes, carboxylic acid esters, and phenols. Both structural and spectroscopic evidence indicate that hydrogen bonding interaction between the triazole residues resulting from the "click" reaction promotes axial ligand binding into the sterically demanding distal pocket in preference to the open proximal side. An iron porphyrin complex with four ferrocene groups is found to bind O_2 and quantitatively reduce it by one electron to O_2^- in apolar organic solvents. However the same complex electro-catalytically reduces O_2 by four electrons to H_2O in aqueous medium under fast, moderate, and slow electron fluxes. This selectivity for O_2 reduction is governed by the reduction potential of the electron transfer site (i.e., ferrocene) which in turn is governed by the solvent. This catalyst mimics control of catalysis of an enzyme active site by a second sphere electron transfer residue which is often encountered in naturally occurring metalloenzymes.

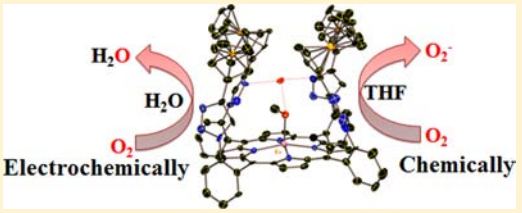

1. INTRODUCTION

Heme based cofactors are abundant in nature. They catalyze fundamentally important transformations in nature, for example, O_2 binding, C−H bond hydroxylation, NO and N_2O formation, and so forth.[1−4] The porphyrin macrocycle of the heme ligand provides a dianionic square planar ligand field and is stable toward oxidation which allows stabilization of highly oxidizing species like Compound I of cytochrome P450.[1,5] Inspired by their diverse reactivities, chemists have pursued synthetic porphyrin systems in the search of functional small molecule catalysts.[6] Decades of dedicated research has led to a few significant breakthroughs, for example, synthetic models of oxy-hemoglobin, functional models of Cytochrome C oxidase (CcO), functional model of nitric oxide reductase (NOR),[7−13] and structural model of cytochrome P450.[14−16] Other than these mimics of natural systems, several Fe and Co based porphyrin catalysts and electrocatalysts are reported, and their reactivities have been investigated.[17−20] In addition to these biomimetic small molecule catalysts there are several reports of zinc porphyrins covalently bonded with ferrocene groups which may act as photovoltaic devices.[21,22]

In most transition metal active sites catalyzing processes that require protons as well as electrons, the electrons are generally stored in adjacent electron transfer (ET) sites, for example, the reductase component of soluble methane monooxygenase, Rieske site in Rieske dioxygenates,[23−25] type I copper sites in multicopper oxidases and nitrite reductases,[26] P-cluster in Nitrogenases, and so forth.[27,28] It is well established that electron transfer properties (both thermodynamic and kinetic) of these sites play a major role in catalysis.[29−32] It is also well-known that the reduction potential of an active site can be tuned by hundreds of milivolts such that it can participate in high potential as well as low potential processes without altering its geometry significantly.[33,34] Several factors are known to affect the reduction potential of these electron transfer sites, for example, solvation, hydrogen bonding, local dielectric, and so forth.[35−37]

In a recent report we have described a novel "click" chemistry based approach to synthesize porphyrin ligands bearing four ferrocene substituents in a hydrogen bonding distal environment.[38] The iron porphyrin was found to selectively reduce O_2 to H_2O in aqueous environment under both fast and slow electron transfer flux from the electrode.[38] In yet another study we have reported that this distal hydrogen bonding pocket enables stabilization of a hydrogen bonded Fe−O_2 adduct.[67] In this paper we investigate O_2 reduction by a series of Fe porphyrins with and without covalently attached ferrocene groups under both homogeneous (in organic solvents) and heterogeneous (in aqueous solvent) conditions. The relevant species and intermediates involved have been characterized using electron paramagnetic resonance (EPR) and resonance Raman (rR) spectroscopy. The results indicate that this catalyst can act as a selective $1e^-$ or $4e^-/4H^+$ reducing catalyst depending on the solvent. This system utilizes the tunability of the reduction potential of the electron donating ferrocene groups to attain selectivity in catalysis.

2. MATERIALS AND METHODS

Tetramethylsilyl azide was purchased from AVRA pvt. Ltd., *t*-butyl nitrite was purchased from MERCK, and all other reagents, for example, ethynyl ferrocene, 2-nitrobenzaldehyde, pyrrole, sodium

Received: October 6, 2012
Published: January 10, 2013

dx.doi.org/10.1021/ic3021782 | *Inorg. Chem.* 2013, 52, 1443−1453

ascorbate, were purchased from Sigma Aldrich (U.S.A.). *t*-Butanol, acetonitrile, dichloromethane, Na_2SO_4, $CuSO_4$ were purchased from MERCK (Germany). Unless otherwise stated all chemicals were used as purchased, and reactions were performed at room temperature. Au (III) wafers were bought from Platypus Technologies (1000 Å of Au on 50 Å of Ti adhesion layer on top of a Si (III) surface. Au discs and Edge Plane Graphite (EPG) discs were purchased from Pine Instruments. The absorption spectra were measured in a Agilent spectrophotometer (model 8453) fitted with a diode array detector. The FT-IR data were measured on a Shimadzu FT-IR 8400S instrument. All the NMR spectra were recorded on a Bruker DPX-300 or a Bruker DPX-500 spectrometer at room temperature. The EPR spectra were recorded on a JEOL instrument. The mass spectra were recorded on a QTOF Micro YA263 instrument. X-ray single crystal data were collected at 120 K using a SMART APEX X-ray diffractometer equipped with CCD detector. Data collection, data reduction, structure solution refinement were carried out using APEX II. The structure was solved by direct method and refined in a routine manner. The non-hydrogen atoms were treated anisotropically. All the hydrogen atoms were located on a difference Fourier map and refined. Resonance Raman (rR) data were collected using 413.1 nm excitation from a Kr^+ ion source (Coherent Inc.) and a Trivista 555 triple spectrophotometer (gratings used in the three stages were 900, 900, and 1800 grooves/mm) fitted with an electronically cooled Pixis CCD camera (Princeton Instruments). The irradiation power was limited to 10 mW at the sample to avoid degradation. Data were collected at room temperature for 200 s.

2.1. Synthesis. The complexes are synthesized as reported.[38]

2.2. Electrochemical Measurements. *2.2.1. Cyclic Voltammetry.* The cyclic voltammograms were recorded on a PAR instrument potentiostat/galvanostat model 237A. A 2 mm diameter Pt electrode was used as a working electrode. A Pt wire was used as a counter electrode. The measurements were made against an Ag/AgCl aqueous reference electrode with scan rates varying from 50 mvs to 500 mvs, pH 7 phosphate buffer, containing 100 mM Na_2HPO_4 and 100 mM KPF_6, has been used as solvent in case of all heterogeneous experiments until otherwise mentioned.

2.2.2. Fabrication of the α_4-FeFc$_4$ (6a) Physiabsorbed Electrodes. a. On Edge Plane Graphite (EPG). A 50 μL portion of a dilute solution (1 mM) of the catalyst (in $CHCl_3$) was uniformly distributed on the disc. After the $CHCl_3$ had evaporated, the surface was sonicated in ethanol for 30 s and washed with triple distilled water.

b. On Alkyl Thiol Self Assembled Monolayer (SAM). Freshly cleaned Au discs and wafers were immersed in ethanolic solutions of C_8SH or $C_{16}SH$ (0.1 mM) for 24 h. These modified surfaces were cleaned with ethanol and water and dried in N_2 gas. The wafers were inserted in the Plate Testing Material and the discs were then mounted in the Pt ring assembly for further experiments. A 50 μL portion of a dilute solution (1 mM) of the catalyst (in $CHCl_3$) was uniformly distributed on the alkyl thiol SAM. After the $CHCl_3$ has evaporated, the surface was sonicated with ethanol and washed with triple distilled water.

2.2.3. Rotating Ring Disc Electrochemistry (RRDE). The RRDE measurements were performed on a CHI 700D bipotentiostat with a Pine Instruments Modulated Speed Rotor. The Au and the Pt surfaces were cleaned with 1 μ, 0.3 μ, and 0.05 μ sized alumina powder before cleaning them electrochemically by repeated sweeping between 1.5 V to −0.3 V in 0.5 M H_2SO_4 at 250 mv/s. The collection efficiency (CE) of the RRDE setup was measured in a 2 mM $K_3Fe(CN)_6$ and 0.1 M KNO_3 solution where $K_3Fe(CN)_6$ was reduced at the Au disc and the Pt ring (which was held at a positive potential) reoxidized it back. An average collection efficiency of 20 ± 2% was generally recorded at 300 rpm. The H_2O_2 was detected by holding the Pt ring at 700 mV vs Ag/AgCl and rotating the electrode at 300 rpm.[39,40] The current detected at the ring was normalized by the collection efficiency determined before or after the RRDE experiments.

2.3. H_2O_2 Assay. *2.3.1. H_2O_2 Generation.* A 1.67 mg portion of α_4-FeFc$_4$ (**6a**) catalyst was dissolved in 1 mL of dry degassed tetrahydrofuran (THF) solvent so that the final strength was 1 mM. A 2.4 mg portion of Na_2S was dissolved in minimum volume of methanol and diluted with dry degassed THF to make the final volume 1 mL, so that the final strength was 10 mM. THF was rigorously degassed using the freeze pump thaw technique. Next, in a glovebox, 100 μL of this solution was added to an EPR tube and 1 equiv(10 μL) of Na_2S was added. It has been recently shown that in a nonpolar organic solvent Na_2S can reduce Fe^{III} porphyrin to Fe^{II} porphyrin and itself gets oxidized to elemental sulfur in the process.[41] The reduction of the Fe by Na_2S was confirmed by EPR and UV−vis absorption. Next, oxygen gas was bubbled through the solution in EPR tube. This sample was subjected to H_2O_2 assay.

2.3.2. H_2O_2 Detection. A xylenol orange assay was used to detect H_2O_2 produced during O_2 reduction under homogeneous conditions.[42] A 4.9 mg portion of Mohr's salt and 3.9 mg of xylenol orange were dissolved in 5 mL of 250 mM H_2SO_4 and stirred for 10 min. A 200 μL portion of this solution was taken in 1.8 mL of triple distilled water, and a calibration curve for quantitative estimation of H_2O_2 was obtained by adding 20 μL aliquots of H_2O_2 having different concentrations and recording their absorbance at 560 nm. The concentrations of H_2O_2 used were 0.05 μM, 0.1 μM, 0.5 μM, 1 μM, 2.5 μM, 5 μM, 10 μM, and 100 μM.

A 200 μL portion of the xylenol orange H_2SO_4 mixture was added to 1.8 mL of H_2O in a cuvette, and the absorbance was recorded. A 100 μL portion of 1 mM reduced α_4-FeFc$_4$ (**6a**) or Fe-"picket fence" (1 mM oxidized α_4-FeFc$_4$ (**6a**) or Fe-"picket fence" in $CHCl_3$/THF + Na_2S (10 μL of 10 mM in CH_3OH)) in an organic solvent ($CHCl_3$/THF) was exposed to dry O_2 gas. This solution was then extracted with 200−400 μL of H_2O. Twenty microliters of this aqueous extract was added to the cuvette containing the xylenol orange and H_2SO_4 mixture. Absorbance for this was recorded. The absorbance of the above solution (after subtracting the control) at 560 nm is fitted in the calibration curve (obtained as described above) to get the corresponding H_2O_2 concentrations. This concentration is scaled accounting for dilution to get the concentration of H_2O_2 produced in the original α_4-FeFc$_4$ (**6a**) solution. Addition of 20 μL of the catalyst solution in THF to the xylenol orange and H_2SO_4 mixture did not result in increase of absorbance at 560 nm.

3.. RESULTS

3.1. Synthesis. The general synthetic protocol is shown in Scheme 1. The synthesis of the catalyst uses 1,3-cycloaddition of aromatic azide to terminal alkyne; also known as "click" reaction. The details are published elsewhere.[38]

3.2. Structure of α_4-ZnFc$_4$ (4a). The structure of the α_4-ZnFc$_4$ (**4a**) complex has been previously reported, and it shows that the Zn metal is in a square pyramidal coordination environment where the four pyrrolic nitrogens of the porphyrin ligand form the equatorial plane and one solvent molecule (methanol) acts as the fifth axial ligand (Figure 1, left).[38] In a conventional "picket fence" type architecture, where the distal pocket is created using amide linkages, the axial ligands generally bind the metal center from the open side, that is, the sterically undemanding proximal side.[43,45] In fact, the crystal structure of an analogous methanol bound tetra(ferrocenyl) zinc porphryin having a "picket fence" type structure (i.e., amide linkages, α_4-ZnPfFc$_4$) shows methanol binding to the open proximal side (Figure 1, right).[44] Thus, to bind O_2 inside the sterically congested distal hydrophobic pocket, the open side has to be blocked using a ligand like imidazole.[43] But the crystal structure of the α_4-ZnFc$_4$ (**4a**) complex (Figure 1, left), bearing a hydrogen bonding hydrophilic triazole distal pocket, shows that even in the absence of any ligand in the open side, the solvent molecule prefers binding to the sterically hindered side because of stabilization by hydrogen bonding interaction with the H_2O molecule held in the cavity by H-bonding with the nitrogen atoms of the triazole rings. Such preference for axial ligand binding into the sterically congested distal side

dx.doi.org/10.1021/ic3021782 | *Inorg. Chem.* 2013, 52, 1443−1453

Scheme 1. (a) General Synthetic Protocol for (a) the "Clicked" Porphyrins and (b) the Iron Metalation of "Clicked" Porphyrins

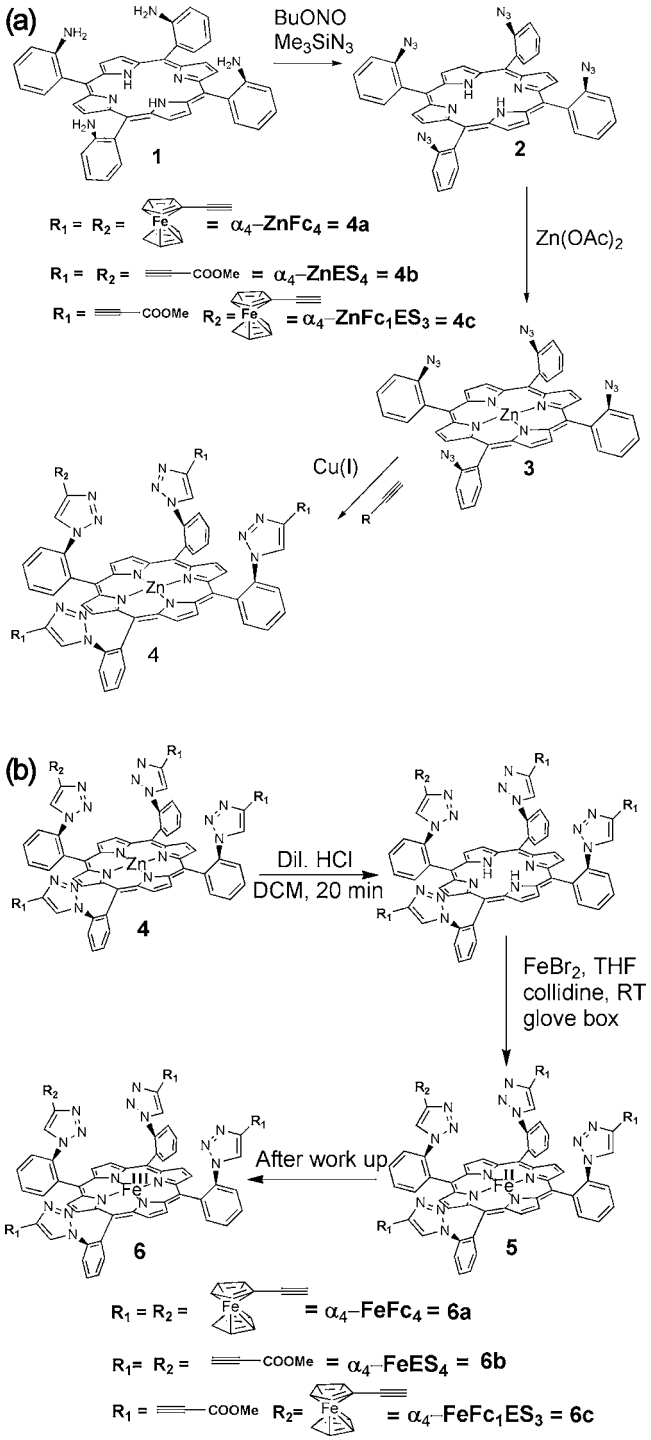

stabilized by hydrogen bonding with H_2O is rarely observed.[45,46]

3.3. Cyclic Voltammetry. Cyclic voltammogram (CV) of the α_4-$FeFc_4$ (**6a**) complex in THF shows three oxidation reduction processes (Figure 2, red).[38] The quasi-reversible wave with $E_{1/2}$ of 0.73 V represents the Fc/Fc^+ couple for the four ferrocene groups in the distal pocket of the α_4-$FeFc_4$ (**6a**) complex. The peak separation between the oxidation and the reduction peaks is ~120−130 mV compared to 120 mV for free ferrocene (Figure 2, blue), clearly indicating that there is no additional interaction between the four ferrocenyl groups as seen in several elegant porphyrin-ferrocene derivatives.[47,48] There is also an quasi-reversible one electron process at 0.98 V. This represents the oxidation of the porphyrin ring (P) to a cation radical species (P^+).[49] Additionally there is another one electron quasi-reversible wave at 0.22 V which represents the $Fe^{III/II}$ couple. In the presence of 2.5 equiv of pyridine in the solution the process observed at 0.22 V shifts to 0.30 V, but the potential for the Fc/Fc^+ and the P/P^+ processes do not change significantly (Figure 2, green). This is consistent with pyridine binding to the heme iron and shifting its thermodynamic reduction potential. CV data of an analogous complex where the Fc groups are replaced by methylester groups (R_1 = R_2= -COOMe in Scheme 1b, α_4-$FeES_4$ (**6b**)) shows the $Fe^{III/II}$ process at 0.26 V in the presence of 2.5 equiv of pyridine in the solution. (Figure 2, black) This value is similar to the value obtained for the α_4-$FeFc_4$ (**6a**) complex. Thus, the fully reduced α_4-$FeFc_4$ (**6a**) complex can donate up to six electrons, one from Fe (Fe^{2+} to Fe^{3+}), one from porphyrin, and one each from four distal ferrocenes, and in principle can act as an O_2 reduction catalyst.

3.4. Homogeneous Single Turnover O_2 Reduction. *3.4.1. Absorption Spectroscopy.* The absorption spectrum of the α_4-$FeES_4$ (**6b**) complex in THF solution shows a Soret band at 422 nm and weaker Q bands at 517 nm, 577 nm, 635 and 681 nm (Figure 3A, black).[38] This complex can be reduced to the all ferrous state in nonpolar dry deoxygenated solvent like THF by the addition of stoichiometric amounts of Na_2S, dissolved in dry degassed methanol.[41] This is indicated by the red shift of the Soret and the Q-band from 422 and 514 nm in the oxidized form (Figure 3A, black) to 428 and 534 nm in the reduced form (Figure 3A, red),[50−52] respectively. Exposing this fully reduced sample to O_2 (maintaining anhydrous conditions) at −80 °C forms a $Fe-O_2$ adduct with the Soret and the Q-bands at 425 and 522 nm, 545 and 584 nm, respectively (Figure 3A, blue).[38]

The absorption spectrum of the α_4-$FeFc_4$ (**6a**) complex shows a Soret band at 424 nm and weaker Q-band at 514 and 670 nm (Figure 3B, black). The reduced complex has the Soret and the Q-band at 433 and 547 nm (Figure 3B, red), respectively. Like the reduced α_4-$FeES_4$ (**6b**) complex, exposing this fully reduced sample to O_2 at −80 °C forms a new species with the Soret and the Q-band at 426 and 543 nm respectively (Figure 3B, green). Addition of 5% H_2O (v:v) to this complex restores the Soret back to as it was for the initial oxidized at 424 cm^{-1}.The Q-bands are however not same as the initial oxidized Fe(III)Fc_4 (**6a**) (Supporting Information, Figure S9) consistent with the EPR data (vide infra).

3.4.2. EPR. The EPR data of the α_4-$FeES_4$ (**6b**) complex, as isolated, shows an axial signal centered around g = 6 indicating that the Fe bound to the porphyrin is in a S = 5/2 Fe(III) state (Figure 4A, black). Reduction of the oxidized complex leads to loss of the high spin Fe(III) EPR signal (Figure 4A, red). Upon exposing the reduced sample to O_2 at −80 °C no new EPR signal is observed suggesting the presence of a diamagnetic O_2 adduct. (Figure 4A, green).[67]

The EPR data of the α_4-$FeFc_4$ (**6a**) complex shows essentially the same trend as the α_4-$FeES_4$ (**6b**) complex, that is, S = 5/2 Fe(III) starting complex (Figure 4B, black), diamagnetic Fe(II) (Figure 4B, red), and oxygen adduct (Figure 4B, green). Note that the crystal structure of the α_4-$ZnFc_4$ (**4a**) shows that the Fe centers in the ferrocenes are in

dx.doi.org/10.1021/ic3021782 | Inorg. Chem. 2013, 52, 1443−1453

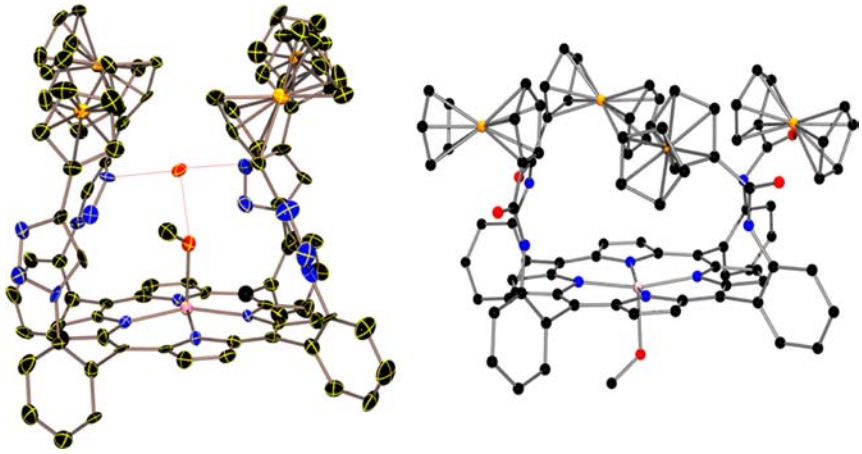

Figure 1. Crystal structure of the α_4-ZnFc$_4$ (**4a**) complex (left) and α_4-ZnPfFc$_4$ complex (right). Carbon atom is shown in black, nitrogen in blue, iron in orange, zinc in pink, oxygen in red. H atoms are omitted. Hydrogen bonding interactions are indicated by pink lines in case of α_4-ZnFc$_4$ (**4a**).

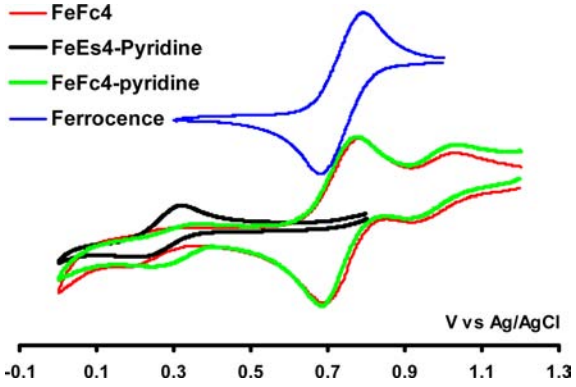

Figure 2. CV of the α_4-FeFc$_4$ (**6a**) complex in THF without (red) and with 2.5 equiv of pyridine (green). The CV of the α_4-FeES$_4$ (**6b**) complex with 2.5 equiv of pyridine (black) and ferrocene (blue) in THF. A Pt working electrode (2 mm diameter), an aqueous Ag/AgCl reference electrode, a Pt counter electrode were used. Data were acquired using a scan rate of 50 mV/s in a THF solution of these complexes having 100 mM tetrabutylammonium perchlorate as the supporting electrolyte.

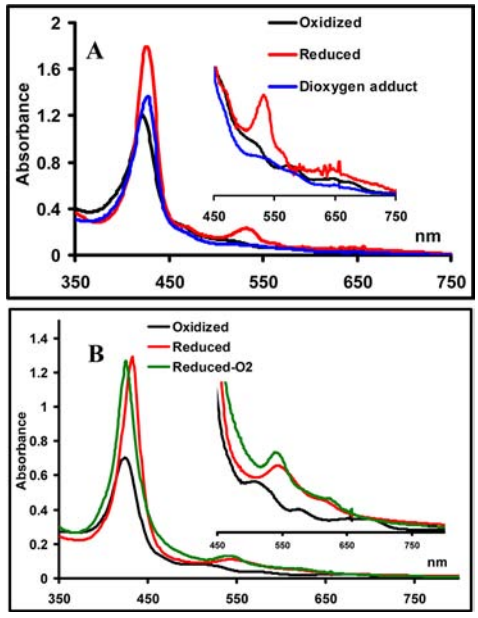

Figure 3. (**A**) Absorption data of the oxidized α_4-FeES$_4$ (**6b**) complex (black). Fully reduced α_4-FeES$_4$ (**6b**) complex (red) and O$_2$ adduct of the α_4-FeES$_4$ (**6b**) complex (blue) at −80 °C, 20 μM in THF. (**B**) Absorption data of the oxidized α_4-FeFc$_4$ (**6a**) complex (black). Fully reduced α_4-FeFc$_4$ (**6a**) complex (red) and O$_2$ adduct of the α_4-FeFc$_4$ (**6a**) complex (green) at −80 °C. Concentration of the sample is 20 μM in THF solvent.

their neutral Fe(II) state. Thus the description of the α_4-FeFc$_4$ (**6a**) complex, as isolated, is likely to be Fe^{III}Fc$^{II}_4$. Additionally, presence of 5% H$_2$O in the solvent gives rise to a rhombic S = 5/2 signal (Figure 4B, blue). This suggests the formation of a high spin Fe(III) species different from the starting complex consistent with the UV−vis data.

3.4.3. Resonance Raman (rR). The rR data of the resting α_4-FeFc$_4$ (**6a**) complex indicates that the ν_8, ν_4, and ν_2 bands are at 390 cm^{-1}, 1365.5 cm^{-1}, and 1557.5 cm^{-1}, respectively (Figure 5A, black). These values are characteristic of a S = 5/2 Fe(III) porphyrin species consistent with the EPR data.[53] The reduction of the complex leads to the shift of the ν_8, ν_4, and ν_2 bands to 386 cm^{-1}, 1346.6 cm^{-1}, and 1544.8 cm^{-1} (Figure 5A, red) respectively, which is characteristic of a S = 2 (high-spin) five coordinate Fe(II) porphyrin species.[53,54] On exposing this reduced complex to O$_2$ at −80 °C the ν_8, ν_4, and the ν_2 vibrations shift to 386 cm^{-1}, 1370 cm^{-1}, and 1565 cm^{-1},(Figure 5A, green dotted line) respectively. It also shows a new band at 585 cm^{-1} (Figure 5B, green) which shifts to 561 cm^{-1}(Figure 6B, green dotted line) on using ^{18}O$_2$ which can be assigned to a Fe−O$_2$ stretch. This is consistent with the formation of a diamagnetic, low-spin, six-coordinate (possibly with a CH$_3$OH as the trans axial ligand) iron oxygen adduct.[55−57] Addition of 5−10% of H$_2$O to the THF solution of this species resurrects a rhombic high spin Fe(III) EPR signal (Figure 4B, blue) indicating hydrolysis of the Fe(III)-O$_2^-$ species generating a high-spin (S = 5/2) Fe(III) porphyrin species. The ν_8, ν_4, and the ν_2 bands for this complex are at 389 cm^{-1}, 1363.6 cm^{-1}, and 1555.8 cm^{-1}, respectively, which indicates formation of a high-spin Fe^{III} porphyrin complex, consistent with the EPR data.[53]

rR data of the α_4-FeES$_4$ (**6b**) catalyst (oxidized) shows that the oxidation and spin state marker ν_4 and the ν_2 bands are at 1361 cm^{-1} and 1555 cm^{-1}, respectively (Figure 6A, black), which are typical of S = 5/2 Fe(III) porphyrins, consistent with the EPR data (Figure 4A, black). Upon reduction these bands shift to 1342 cm^{-1} and 1542 cm^{-1}, indicating formation of a high-spin S = 2 Fe(II) species (Figure 5A, red). The O$_2$ adduct,

dx.doi.org/10.1021/ic3021782 | Inorg. Chem. 2013, 52, 1443−1453

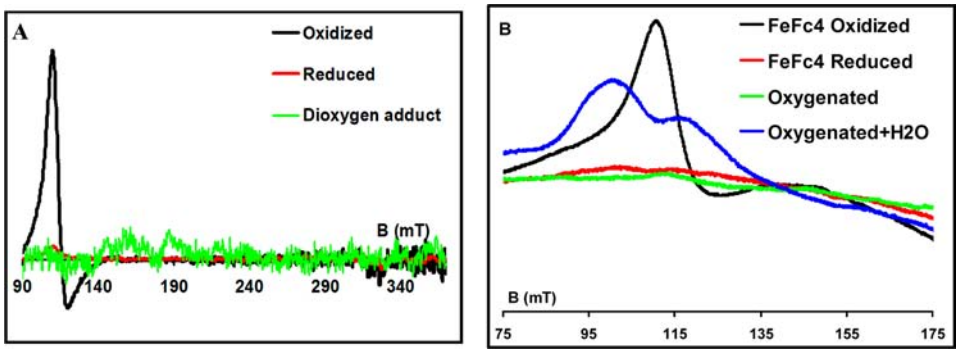

Figure 4. (A) EPR data of the, as isolated, α_4-FeES$_4$ (**6b**) complex (black), fully reduced α_4-FeES$_4$ (**6b**) complex (red), O_2 adduct of the α_4-FeFc$_4$ (**6b**) complex (green). Concentration of sample = 1 mM in THF, T = 77 K.[38] (**B**) EPR data of the, as isolated, α_4-FeFc$_4$ (**6a**) complex (black), fully reduced α_4-FeFc$_4$ (**6a**) complex (red), O_2 adduct of the α_4-FeFc$_4$ (**6a**) complex (green), and the product after H_2O addition to the O_2 adduct of the α_4-FeFc$_4$ (**6a**) complex (blue). Concentration of sample = 1 mM in THF, T = 77 K.

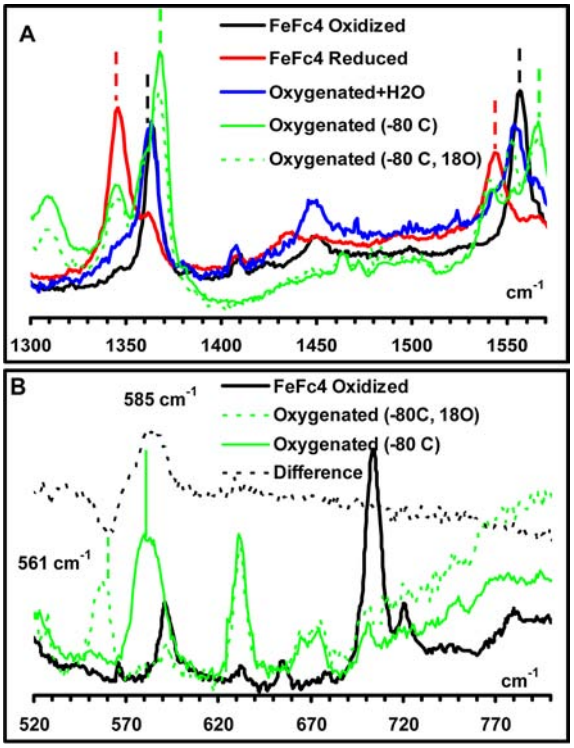

Figure 5. (**A**) rR data of the as isolated α_4-FeFc$_4$ (**6a**) complex (black), the fully reduced α_4-FeFc$_4$ (**6a**) complex (red), the oxygen adduct (green, note some of the reduced complex is still present as indicated by the presence of a weak ν_4 band at 1346 cm^{-1}), and the final product (blue). (**B**) the rR data of α_4-FeFc$_4$ (**6a**) complex in the 500−800 cm^{-1} region. Samples are 1 mM in THF, λ = 413.1 nm, 77 K, Laser power =10 mW.

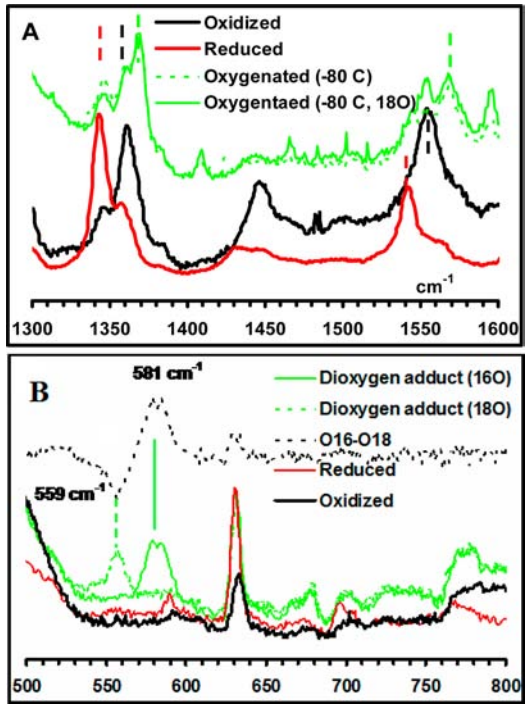

Figure 6. (**A**) rR data of the as isolated α_4-FeES$_4$ (**6b**) complex (black), the fully reduced α_4-FeES$_4$ (**6b**) complex (red), the oxygen adduct (green, note some of the reduced complex is still present as indicated by the presence of a weak ν_4 band at 1346 cm^{-1}), and the final product (blue). (**B**) The rR data of the above complexes in the 500−800 cm^{-1} region. Samples are 1 mM in THF, λ = 413.1 nm, 77 K, Laser power = 10 mW.

in addition to some residual Fe(II) and Fe(III) signals, shows a new set of bands at 1369 cm^{-1} and 1568 cm^{-1} (Figure 6A, green). This is characteristic of six-coordinate heme Fe−O_2 adducts where the Fe center is in a low-spin S = 1/2 Fe(III) state. The rR data of the O_2 adduct in the 500−800 cm^{-1} region show a Fe−O vibration at 581 cm^{-1} (Figure 6B, green) which shifts to 559 cm^{-1} (Figure 6B, green dotted line) on substituting with $^{18}O_2$. Thus, in conjunction with the EPR data and the ν_4 and ν_2 bands in the rR spectra, the observation of the Fe−O vibration at 581 cm^{-1} is consistent with the formation of a six coordinate end-on S = 0 Fe−O_2 adduct.[38]

Note that the binding of O_2 in the open side of the α_4-FeFc$_4$ (**6a**) or α_4-FeES$_4$ (**6b**) complex would have led to the formation of an antiferromagnetically coupled S = 0 μ-oxo dimer.[58,59] The EPR silent μ-oxo dimer of the α_4-FeFc$_4$ (**6a**) complex (Supporting Information, Figure S6A), synthesized according to reported procedures, spectroscopic features distinct from the oxy adduct as well as the starting complex (Fe^{III}Fc$_4$)(**6a**).[60] In particular the bands at 365 and 508 nm in the absorption spectrum of Fe^{III}Fc$_4$ shift to 336 and 582 nm, respectively, in the μ-oxo-dimer (Supporting Information, Figure S6B). The rR data of the μ-oxo dimer shows the presence of five coordinate high spin Fe(III) species, different

dx.doi.org/10.1021/ic3021782 | Inorg. Chem. 2013, 52, 1443−1453

Scheme 2. Mechanism of O_2 Reduction by the α_4-$FeFc_4$ (6a) Complex in THF

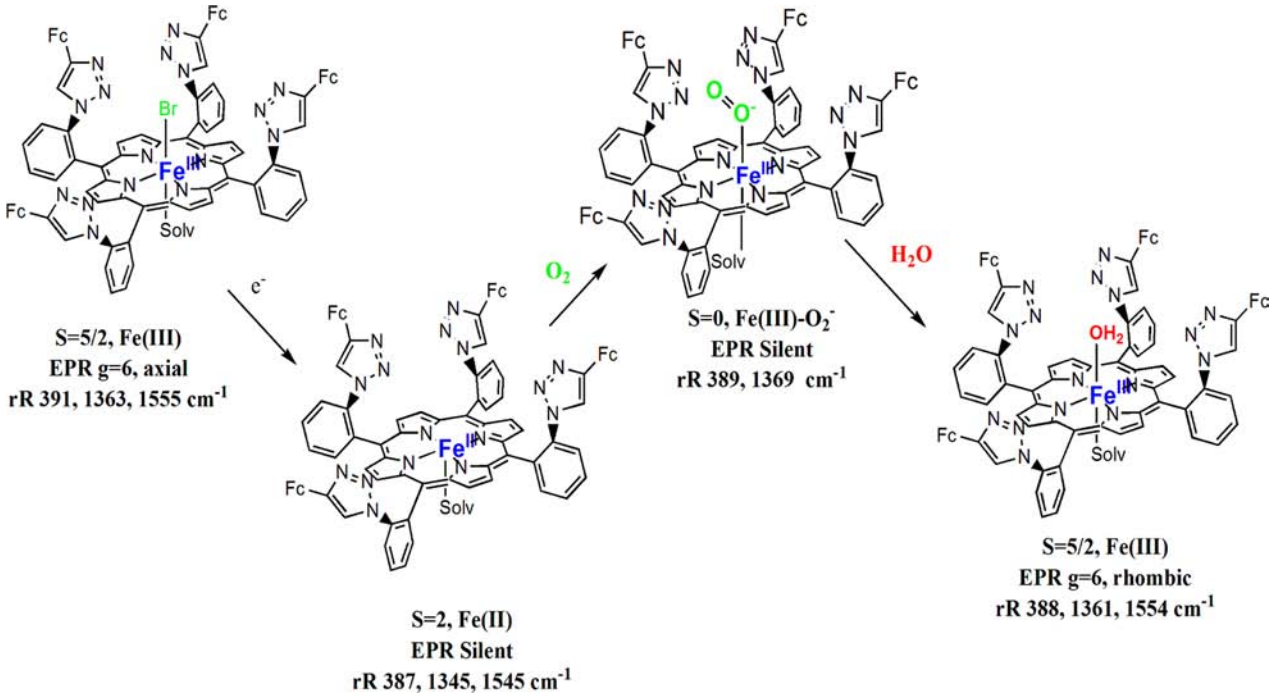

from the six coordinate low spin species observed in the oxy intermediate (Supporting Information, Figure S6C and S6D).

The fact that a μ-oxo dimer is not formed on exposing the reduced complex to O_2 and the H/D isotope effect in the O−O vibration observed for the analogous $FeES_4$(**6b**) complex suggests that the O_2 binds inside the cavity.[67] The hydrogen bonding network that drives the methanol molecule to bind inside the distal pocket, as observed crystallographically in the α_4-$ZnFc_4$ (**4a**) complex, possibly results in O_2 binding inside this distal pocket of the α_4-$FeFc_4$ (**6a**) complex as well, avoiding formation of the μ-oxo-dimer.

O_2 can be reduced by one electron to O_2^- or by two electrons to H_2O_2 or by four electrons to H_2O. In these cases H_2O_2 was detected in 48 ± 3% yield in the resultant solution using a xylenol orange assay. This indicates that in spite of having six electrons, the α_4-$FeFc_4$ (**6a**) catalyst selectively reduces O_2 to O_2^- and not H_2O in a nonpolar organic solvent. The Fe−O_2 adduct (observed in absorption and EPR) is hydrolyzed by H_2O to release O_2^- which then disproportionate to H_2O_2 and O_2 yielding an overall 50% H_2O_2. The reactivity of the α_4-$FeFc_4$ (**6a**) complex in THF is summarized in Scheme 2.

3.5. Heterogeneous Electrocatalytic O_2 Reduction. *a). On Edge-Plane Graphite Surface.* Rotating disc electrochemistry (RDE) is a convenient approach for analyzing electrocatalytic currents using the Koutecky−Levich equation (Figure 7).[40]

$$I^{-1} = i_K(E)^{-1} + i_L^{-1}$$

where $i_K(E)$ is the potential dependent kinetic current, i_L is the Levich current given by

$$i_L = -0.62nFA[O_2](D_{O2})^{2/3}\omega^{1/2}\nu^{1/6}$$

where n is the number of electrons transferred to the substrate, A is the macroscopic area of the disc (0.096 cm^2), $[O_2]$ is the concentration of O_2 in an air saturated buffer (0.26 mM) at 25 °C, D_{O2} is the diffusion coefficient of O_2 (1.8×10^{-5} cm^2 s^{-1})

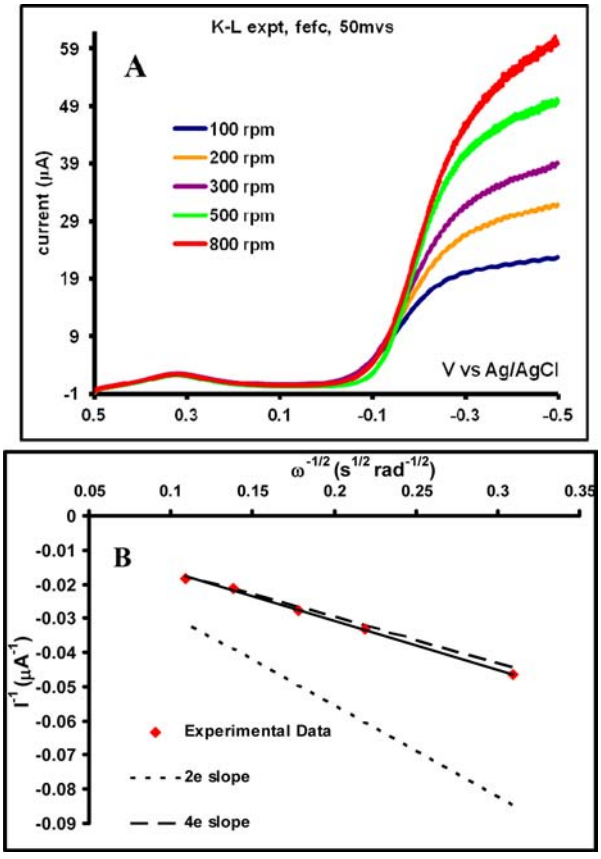

Figure 7. (**A**) LSV of α_4-$FeFc_4$ (**6a**) deposited on EPG surface at multiple rotations. pH = 7, 100 mM KPF_6. (**B**) K-L plot of the α_4-$FeFc_4$ (**6a**) catalyst (black bold line). The short and the long dashed lines indicate the theoretical plots for $2e^-$ and $4e^-$ transfers respectively.

dx.doi.org/10.1021/ic3021782 | Inorg. Chem. 2013, 52, 1443−1453

at 25 °C,[61] ω is the angular velocity of the disc, and ν is the kinematic viscosity of the solution (0.009 $cm^2\ s^{-1}$) at 25 °C.[62]

Linear sweep voltammetry (LSV) of the α_4-$FeFc_4$ (**6a**) catalyst shows a catalytic O_2 reduction current which shows substrate diffusion limited current at negative potentials. This O_2 reducing potential coincides with the Fe^{III}/Fe^{II} couple (vide infra). Note that the Fc^+/Fc reductive process is observed at 0.305 V.[38] RDE of the α_4-$FeFc_4$ (**6a**) catalyst show that the catalytic current increases with angular rotation frequency. Plot of I^{-1} at multiple rotation rates with the inverse square root of the angular rotation rate ($\omega^{-1/2}$) is linear. The slope obtained from the experimental data is almost identical to that predicted for a $4e^-$ process (Figure.7B) and very different from that predicted for a $2e^-$ process (Figure 7B). The experimentally obtained slope indicates an $n = 3.88$ for the process, that is, 97% of O_2 is reduced to H_2O. Thus in contrast to the results obtained in organic solvents where a 1 e^- reduction of O_2 to O_2^- is facilitated by the α_4-$FeFc_4$ (**6a**) catalyst, a $4e^-$ reduction is favored in the aqueous medium.[38]

Unfortunately, the α_4-$FeES_4$ (**6b**) complex could not be successfully adsorbed on EPG surfaces. However similar experiments were also performed with a complex where only one of the four −COOMe groups of α_4-$FeES_4$ (**6b**) complex is replaced by a ferrocene group (α_4-$FeFc_1ES_3$ (**6c**) complex). The K-L data (Figure 8, A and B) of the α_4-$FeFc_1ES_3$ (**6c**) catalyst indicates that the plot of I^{-1} vs $\omega^{1/2}$ is linear, and its slope agrees with that the theoretical slope for a $4e^-$ process. Thus this catalyst also catalyzes the $4e^-$ reduction of O_2 to H_2O. Thus under fast electron flux both the monoferrocene and the tetraferrocence derivatives selectively reduced O_2 to H_2O. This is not surprising as it is now well-known that, when

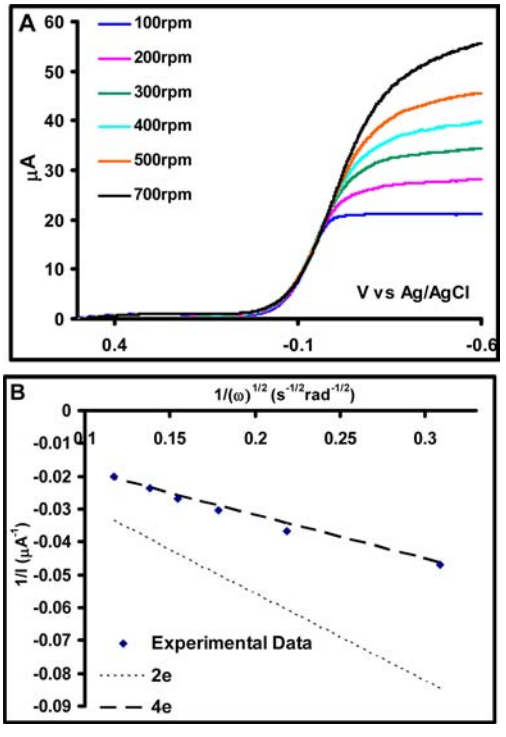

Figure 8. (**A**) LSV of α_4-$FeFc_1ES_3$ (**6c**) deposited on EPG surface at multiple rotations. pH =7, 100 mM KPF_6. (**B**) K-L plot of the α_4-$FeFc_1ES_3$ (**6c**) catalyst (black bold line). The short and the long dashed lines indicate the theoretical plots for $2e^-$ and $4e^-$ transfers respectively.

immobilized on graphite electrodes, species not having enough electrons to reduce O_2 to H_2O can do so by facilitating electron transfer from the electrode to O_2.[46,63]

The intercept of the K-L plot is the inverse of the kinetic current ($i_K(E)^{-1}$) where $i_K(E)$ is expressed as

$$i_K(E) = k_{cat} nF[O_2]\Gamma_{cat}$$

where n is the number of electron, $[O_2]$ is the bulk concentration of O_2, Γ_{cat} is the surface coverage of the catalyst (obtained from the integration of the anaerobic CV data), and k_{cat} is the second order rate constant for O_2 reduction. Using this equation and the experimentally obtained i_K at −400 mV, the second order rate constant for O_2 reduction by α_4-$FeFc_1ES_3$ (**6c**) and α_4-$FeFc_4$ (**6a**) at pH 7 are obtained to be $5 \pm 1 \times 10^4$ and $7 \pm 2 \times 10^4\ M^{-1}\ s^{-1}$, respectively. These values are similar to values reported for other Fe porphyrin catalysts at this pH.[39]

b.) On Self-Assembled Monolayers of Varying Chain Lengths on Au Surfaces. The electrocatalytic O_2 reduction by these catalysts are also evaluated by physiabsorbing the catalyst on an alkane thiol self-assembled monolayer (SAM) on Au electrode. The resultant surface was characterized with surface enhanced rR spectroscopy (SERRS). The data indicate the presence of the α_4-$FeFc_4$ (**6a**) and α_4-$FeES_4$ (**6b**) complexes on the thiol surfaces (Figure 9). The oxidation and spin state

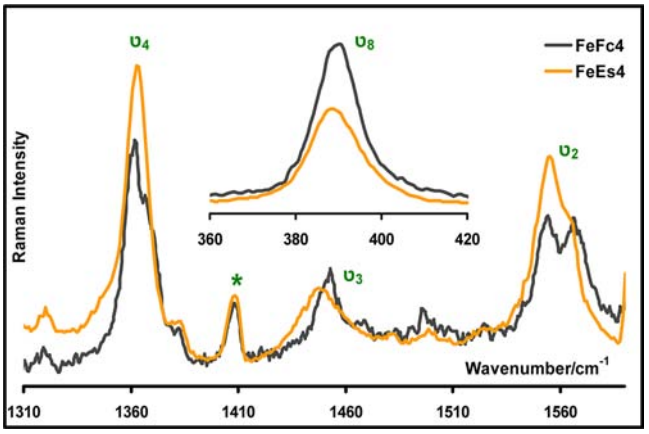

Figure 9. SERRS data of oxidized α_4-$FeFc_4$ (**6a**) (yellow) and α_4-$FeES_4$ (**6b**) (black) physiabsorbed on C_8SH modified roughened Ag disc in pH 7 buffer.

marker ν_4, ν_3, and ν_2 bands for the α_4-$FeFc_4$ (**6a**) complex are 1363 cm^{-1}, 1450 cm^{-1}, and 1556 cm^{-1}, respectively. These values suggest the presence of high spin ferric species on these surfaces. Note that there is a shoulder at 1565 cm^{-1} which indicates the presence of some low spin component. In contrast the SERRS data of the α_4-$FeES_4$ (**6b**) complex show a clear mixture of high spin and low spin species with the oxidation and spin state marker ν_4 and ν_3 bands at 1363 cm^{-1} and 1555 cm^{-1} and 1367 cm^{-1} and 1565 cm^{-1}, respectively.

CV of an Au wafer coated with octane thiol SAM with the catalyst physiabsorbed on it, in the presence of O_2, shows the Fc/Fc^+ process at 0.37 V and the electrocatalytic O_2 reduction peaking at −300 mV (Figure 10A). The integration of the Fc/Fc^+ current indicates that about $(1-5) \times 10^{12}$ molecules of α_4-$FeFc_4$ (**6a**) complex are physiabsorbed per square cm area on the electrode in different preparations. Since the surface coverage of a thiol SAM is $\sim 10^{14}$ molecules/cm^2, this indicates that physiabsorption produces a dilute layer of catalyst with 1−5% surface coverage. In absence of O_2 the Fe^{III}/Fe^{II} couple can

dx.doi.org/10.1021/ic3021782 | Inorg. Chem. 2013, 52, 1443−1453

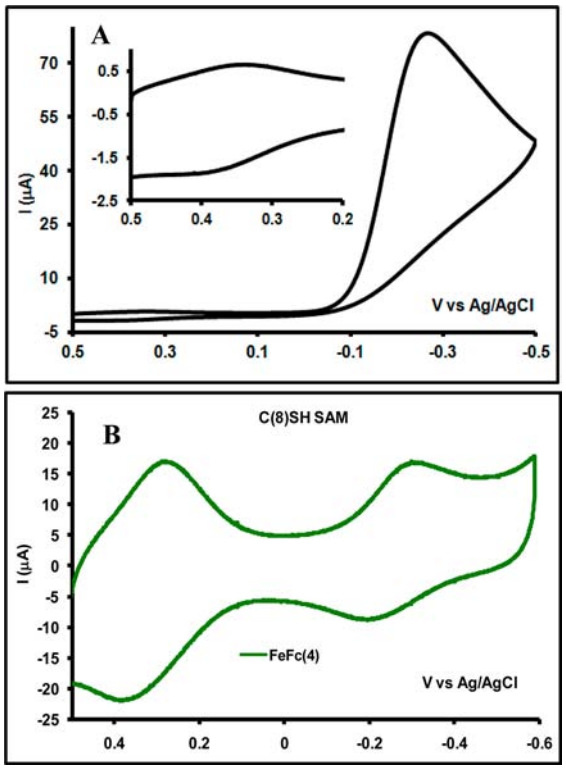

Figure 10. CV of the α_4-$FeFc_4$ (**6a**) functionalized Au electrodes in air saturated pH 7 (A) and degassed Ar saturated pH 7(B) buffers at scan rates of 50 mV/s and 1 V/s, respectively, using Pt counter electrode, Ag/AgCl reference electrode. The Fc/Fc^+ CV has been enlarged and shown as an inset in (A).

be observed (Figure 10B) at a potential of −252 mV. Note that the Fe^{III}/Fe^{II} CV coincides well with the onset-potential of O_2 reduction current. A normal K-L analysis of the electrocatalytic O_2 reduction could not be done owing to weak physiabsorption of the α_4-$FeFc_4$ (**6a**) catalyst on the thiol monolayer. However the generation of H_2O_2 during O_2 reduction can be quantitatively demonstrated in the RRDE experiments, and the amount of H_2O_2 generated indicates the selectivity of the catalyst toward $2e^-$ or $4e^-$ O_2 reduction.[8]

In a RRDE experiment using an Au disc covered with octane thiol SAM with the catalyst physiabsorbed on it, partially reduced oxygen species (PROS), for example, H_2O_2 produced because of partial reduction of O_2, is detected in situ by the Pt ring which encircles the disc and is held at a constant potential where it oxidizes H_2O_2 to O_2. This technique has been applied to investigate electrocatalytic O_2 reduction by the α_4-$FeFc_4$ (**6a**) complex as well as by the α_4-$FeES_4$ (**6b**) and α_4-$FeFc_1ES_3$ (**6c**) complexes as control (Scheme 1b). The α_4-$FeES_4$ (**6b**) complex contains four triazoles (resulting from clicking propynoic acid methyl ester to TAzPP) but no electron donating Fc groups and serves as an appropriate reference complex. This complex produces 28 ± 4% H_2O_2 (Table 1), that is, only 72% of the O_2 is reduced to H_2O. Note that the α_4-$FeES_4$ (**6b**) does not have the necessary number of electrons to reduce O_2 to H_2O, that is, 100% H_2O_2 should form. The electrode directly provides these additional electrons needed for O_2 reduction. Introduction of one ferrocene electron donor site in the α_4-$FeFc_1ES_3$ (**6c**) complex reduces the amount of H_2O_2 to 16 ± 2% (Table 1), that is, 84% of O_2 is reduced to H_2O. The amount of H_2O_2 produced by the α_4-$FeFc_4$ (**6a**)

Table 1. H_2O_2 Produced by the Fe Complexes Immobilized on Alkanethiols

	H_2O_2	
complex	C_8SH	$C_{16}SH$
α_4-$FeFc_4$ (**6a**)	2 ± 1	10
Fe-"picket fence"	10 ± 1	rapid degradation
α_4-$FeES_4$ (**6b**)	28 ± 4	~100
α_4-$FeFc_1ES_3$ (**6c**)	16 ± 2	42 ± 2

catalyst during O_2 reduction is only 1−2% (Table 1), that is, 97−99% of O_2 is converted to H_2O. Thus both the RRDE experiments on SAM modified Au electrodes and the K-L analysis on EPG discs reveal that the α_4-$FeFc_4$ (**6a**) complex reduces >97% of O_2 to H_2O in an aqueous medium. The above data show a clear trend of increasing selectivity for the $4e^-$ O_2 reduction as the number of electron donating ferrocene groups is increased. However, as mentioned above, direct electron transfer from the electrode during the electrocatalytic O_2 reduction by these catalysts may jeopardize appraisal of the contribution from the ferrocenes toward the observed increase in selectivity.

The electron transfer rate from the electrode to the catalyst is greatly reduced by extending the chain length of the thiols used to prepare the SAM, for example, octanethiol (500 s^{-1}) to hexadecanethiol (4−6 s^{-1}).[64] RRDE experiments physiabsorbing the α_4-$FeES_4$ (**6b**) complex on a hexadecanethiol SAM produce 100% H_2O_2 (Table 1). This indicates that in this case the production of H_2O_2 is much faster than electron transfer from the electrode. Thus under sluggish electron flux the electrode fails to supply the additional electrons needed for complete O_2 reduction by the α_4-$FeES_4$ (**6b**). This, in effect, mimics homogeneous catalysis where no additional sources of electrons, other than the ones already present in the catalyst, are available. The α_4-$FeFc_1ES_3$ (**6c**) complex produces 42 ± 2% H_2O_2 (Table 1) which is significantly lower than the quantitative H_2O_2 produced by the α_4-$FeES_4$ (**6b**) complex which did not have an additional electron donor site. The α_4-$FeFc_4$ (**6a**) catalyst, which has four electron donor site, produces 11.5 ± 0.5% H_2O_2 during O_2 reduction (Table 1), that is, 89% of O_2 is reduced to H_2O under slow electron flux. Thus the extra redox centers in the distal pocket (i.e., ferrocene) prevent incomplete O_2 reduction in aqueous environments under fast (edge plane graphite), medium (octane thiol), and slow (hexadecane thiol) electron transfer rates. Addition of redox centers are known to increase selectivity of O_2 reduction in functional models of CcO reported by Collman et al.[6,8,39] and Ru modified Co porphyrins reported by Anson et al.[19,65]

4. DISCUSSION

The four triazoles substituents in the distal pocket of these porphyrin ligands provide hydrogen bonding groups like the four amide bonds in a "picket fence" type porphyrin. However the hydrogen bonding by the triazoles[66] are much stronger as substantiated by the crystallographically observed H_2O molecule trapped inside the sterically congested distal pocket (Figure 11, left). A remarkable effect of this hydrogen bonding network in these complexes is the inversion of the axial ligand binding affinity relative to a picket fence porphyrin.[38] In an analogous methanol bound Zn(II) complex of a tetra ferrocene "picket fence" porphyrin α_4-$ZnPfFc_4$ (Figure 11B) steric interaction is overcome by hydrogen bonding interactions

dx.doi.org/10.1021/ic3021782 | Inorg. Chem. 2013, 52, 1443−1453

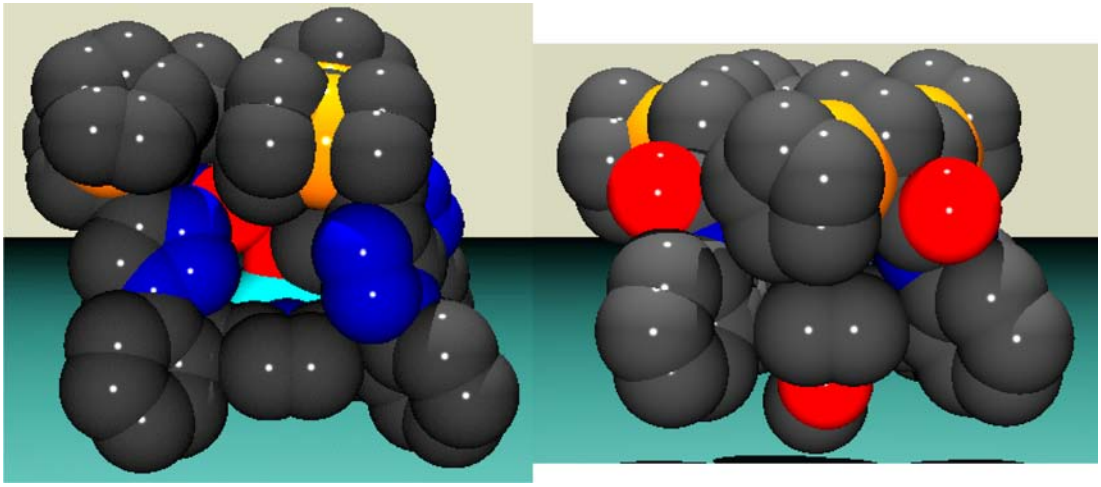

Figure 11. Space filling model of the α_4-ZnFc$_4$ (**4a**) (left) and α_4-ZnPfFc$_4$ (right) complexes. The red spheres at the center of α_4-ZnFc$_4$ (**4a**) indicate the oxygen atoms of the bound CH_3OH and hydrogen bonded H_2O trapped inside the cavity.

with the triazoles and the water molecule. Thus the axial ligand (in this case methanol) and the water molecules are trapped inside the sterically congested distal pocket (Figure 11). This hydrogen bonding network possibly stabilizes the Fe−O_2 adduct.[67] The dioxygen adduct is six coordinated low spin Fe(III) as evident from the NMR and rR data. While the NMR (Supporting Information, Figure S10) of the Fe−O_2 adduct at −50 °C in $CDCl_3$ reveals a broad β-pyrrole resonance at δ = 9.4 ppm, the rR data show a Fe−O_2 vibration at 581 cm^{-1} which are both characteristic of diamagnetic 6-coordinate iron-oxy species.[51,56,68] The rR vibration of Fe−O at 581−585 cm^{-1} are typical for a 6C Fe−O_2 adduct. Recently stabilization of Fe−O_2 adduct using a similar distal hydrogen bonded distal environment has been proposed.[69] In nonheme Fe systems, hydrogen bonding has been used to stabilize very unusual axial ligands.[70] Also note that because of the triazole rings in the α_4-ZnFc$_4$ (**4a**) complex (Figure 11B, left), the hydrophobic ferrocene groups are further away from the Zn atom than they are in the α_4-ZnPfFc$_4$ complex (Figure 11B, right). This results in a more hydrophilic environment in the vicinity of the metal ion in the α_4-ZnFc$_4$ (**4a**) complex relative to the α_4-ZnPfFc$_4$ complex.

The chemically reduced α_4-FeFc$_4$ (**6a**) and the α_4-FeES$_4$ (**6b**) catalysts can bind O_2 and produce stable Fe−O_2 species. In an organic solvent this species is hydrolyzed by H_2O to liberate equivalent amount of superoxide (i.e., half equivalent of H_2O_2). Analogous experiments are performed with iron "picket fence" porphyrin which has no added redox centers, and produces comparable amount of O_2^-. The same is observed when the electrochemically reduced complexes are exposed to O_2. Thus in spite of the presence of additional redox centers, this catalyst can only donate 1e$^-$ to O_2 (i.e., only the Fe(II)-heme gets oxidized and not the ferrocenes). The quantitative production of O_2^-, and not the formation of μ-oxo dimer, upon reaction of the reduced catalyst with O_2, suggests that the O_2 binds inside the sterically congested distal pocket of the α_4-FeFc$_4$ (**6a**) catalyst like CH_3OH binds in the analogous α_4-ZnFc$_4$ (**4a**) complex.

The RDE experiments on EPG disc indicate that the α_4-FeFc$_4$ (**6a**) and α_4-FeFc$_1$ES$_3$ (**6c**) complexes catalyst reduce O_2 by 4e$^-$ to H_2O in pH 7 buffer.[38] As suggested by the rR and EPR data obtained in organic solvent, during the reduction of O_2 by these iron porphyrin catalysts a Fe^{III}−O_2^- adduct is likely to be formed upon O_2 binding to the reduced Fe^{II} formed, on the electrode, in situ.[38] This species can either be further reduced to produce H_2O or hydrolyzed to produce H_2O_2 depending on the relative rates of electron transfer or hydrolysis, respectively. The H_2O_2 produced is detected in the Pt ring electrode during a RRDE experiment. The RRDE experiments on octane thiol SAM on Au discs show that the α_4-FeES$_4$ (**6b**), α_4-FeFc$_1$ES$_3$ (**6c**), and α_4-FeFc$_4$ (**6a**) catalysts produce 28%, 16%, and 2% H_2O_2 under the same conditions. These molecules have the same distal structure (i.e., have 1,2,3-triazole linkages) and only vary in the number of Fc groups (i.e., number of electron donor groups) present. Thus these results clearly indicate that the presence of the additional redox centers increases the selectivity for 4e$^-$ reduction of O_2.

The general oxygen reduction mechanism along with PROS formation by an iron porphyrin catalyst is described in Scheme 3. Under very slow electron flux (i.e., on a hexadecane thiol SAM) the α_4-FeES$_4$ (**6b**) complex produces 100% H_2O_2 indicating that the hydrolysis of the Fe−O_2^- or Fe^{III}−OOH (i.e., steps iii and iv) is much faster than the electron transfer from the electrode, that is, the electrode does not participate in O_2 reduction. Thus under slow electron flux, this heterogeneous construct is practically equivalent to the homogeneous reaction condition where no electrode is present. Under these conditions introduction of one and four electron transfer sites (i.e., the α_4-FeFc$_1$ES$_3$ (**6c**) and the α_4-FeFc$_4$ (**6a**) complex) reduces the H_2O_2 production to 42% and 11%, respectively.

Scheme 3. Oxygen Reduction Mechanism by an Iron Porphyrin

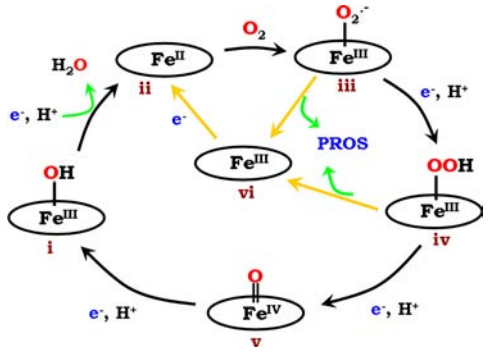

dx.doi.org/10.1021/ic3021782 | Inorg. Chem. 2013, 52, 1443−1453

Thus inclusion of the additional ferrocene redox centers remarkably enhances the $4e^-$ O_2 reduction selectivity (~an order of magnitude; from 100% H_2O_2 in α_4-$FeFc_1ES_3$ (**6c**) to 11% H_2O_2 in the α_4-$FeFc_4$ (**6a**) complex) in the aqueous environment under slow electron flux. This observation concurs with those obtained using functional models of CcO where inclusion of additional redox active sites increase the selectivity for $4e^-$ reduction of O_2.[8]

The α_4-$FeFc_4$ (**6a**) complex reported in this study can selectively reduce O_2 to O_2^- or H_2O. The selectivity is governed by the solvent polarity. In nonpolar solvents EPR, rR, and UV−vis absorption measurements indicate that the O_2 binds to the fully reduced catalyst (chemically as well as electrochemically) and is quantitatively reduced to O_2^-. Alternatively, in aqueous solvents the RDE as well as RRDE experiments show that the O_2 is selectively reduced to H_2O under fast (EPG), medium (octanethiol), and slow (hexadecanethiol) electron flux. This difference in reactivity is due to the shift in the reduction potential of the distal ferrocene groups in different solvents. Proton is available in both aqueous and nonaqueous solvents (10−20% of H_2O was added to THF solutions of the oxygenated catalyst). In a nonpolar organic solvent the Fc/Fc^+ potential is observed at 0.73 V (Figure 2, red). In aqueous environment this potential is lowered by ~0.350 to 0.375 V (on thiol SAM) or 0.305 V (on EPG) (Figure 10, inset). This is due to the enhanced solvation of the charged Fc^+ ion in aqueous medium relative to a nonpolar organic solvent. This enables the oxidation of the Fc centers in an aqueous environment which results in the four electron reduction of O_2 to H_2O.[26,71]

Several metallo-enzymes that catalyze fundamental reactions in nature involve multiple protons and multiple electron transfers, for example, CcO and multicopper oxidases catalyze the $4e^-/4H^+$ reduction of O_2 to H_2O, cytochrome P450 catalyze oxidation of organic substrate after reducing O_2 to peroxide using $2e^-/1H^+$,[1] nitrogenase catalyzes the $6e^-/6H^+$ reduction of N_2, and so forth.[72] In most of these cases the electrons are derived from additional redox active site(s) present in these enzymes distinct from the substrate binding/activating active site. These include heme *a* sites in CcO,[71] ferredoxin site in P450 and P-cluster of Nitrogenase. These metal based electron transfer sites change its charge during the redox process. Thus the reduction potential of these sites can be tuned dramatically by tuning their local environment which may play a fundamental role in tuning the reactivity of their associated catalytic active sites.[33,35,37] The solvent controlled reactivity of the α_4-$FeFc_4$ (**6a**) complex reported here is the first synthetic small molecule analogue of that. Here the solvent controlled reduction potential of the covalently attached electron donating second sphere ferrocenyl moiety determines the selectivity of O_2 reduction by the Fe porphyrin catalyst.

■ ASSOCIATED CONTENT

Supporting Information

Cyclic voltammetry, RRDE, EPR, absorption and resonance Raman, and NMR data. This material is available free of charge via the Internet at http://pubs.acs.org.

■ AUTHOR INFORMATION

Corresponding Author

*E-mail: icad@iacs.res.in.

Author Contributions

[†]These authors contributed equally to this manuscript.

Notes

The authors declare no competing financial interest.

■ ACKNOWLEDGMENTS

This work was funded by the department of science and technology, India (DST/SR/IC-35-2009). S.S. acknowledges the integrated Ph.D. program of IACS. K.S., K.M., and S.C. acknowledge CSIR JRF and SRF fellowships respectively. Dr. Somdatta Ghosh Dey is thanked for her help in preparing the manuscript. Prof. Viktor Nemykin is acknowledged for helpful discussions.

■ REFERENCES

(1) Denisov, I. G.; Makris, T. M.; Sligar, S. G.; Schlichting, I. *Chem. Rev.* **2005**, *105*, 2253−2278.
(2) Averill, B. A. *Chem. Rev.* **1996**, *96*, 2951−2964.
(3) Zumft, W. G. *Arch. Microbiol.* **1993**, *160*, 253−264.
(4) Wasser, I. M.; de Vries, S.; Moenne-Loccoz, P.; Schroder, I.; Karlin, K. D. *Chem. Rev.* **2002**, *102*, 1201−1234.
(5) Shaik, S.; Kumar, D.; de Visser, S. l. P.; Altun, A.; Thiel, W. *Chem. Rev.* **2005**, *105*, 2279−2328.
(6) Collman, J. P.; Boulatov, R.; Sunderland, C. J.; Fu, L. *Chem. Rev.* **2004**, *104*, 561−588.
(7) Collman, J. P. *Acc. Chem. Res.* **1977**, *10*, 265−272.
(8) Collman, J. P.; Devaraj, N. K.; Decreau, R. A.; Yang, Y.; Yan, Y. L.; Ebina, W.; Eberspacher, T. A.; Chidsey, C. E. D. *Science* **2007**, *315*, 1565−1568.
(9) Collman, J. P.; Yang, Y.; Dey, A.; Decreau, R. A.; Ghosh, S.; Ohta, T.; Solomon, E. I. *Proc. Natl. Acad. Sci. U. S. A.* **2008**, *105*, 15660−15665.
(10) Kim, E.; Chufan, E. E.; Kamaraj, K.; Karlin, K. D. *Chem. Rev.* **2004**, *104*, 1077−1133.
(11) Halime, Z.; Kotani, H.; Li, Y.; Fukuzumi, S.; Karlin, K. D. *Proc. Natl. Acad. Sci. U. S. A.* **2011**, *108*, 13990−13994.
(12) Chishiro, T.; Shimazaki, Y.; Tani, F.; Tachi, Y.; Naruta, Y.; Karasawa, S.; Hayami, S.; Maeda, Y. *Angew. Chem., Int. Ed.* **2003**, *42*, 2788−2791.
(13) Liu, J. G.; Naruta, Y.; Tani, F. *Angew. Chem., Int. Ed.* **2005**, *44*, 1836−1840.
(14) Matsu-ura, M.; Tani, F.; Nakayama, S.; Nakamura, N.; Naruta, Y. *Angew. Chem., Int. Ed.* **2000**, *39*, 1989−+.
(15) Matsui, E.; Naruta, Y.; Tani, F.; Shimazaki, Y. *Angew. Chem., Int. Ed.* **2003**, *42*, 2744−2747.
(16) Higuchi, T.; Uzu, S.; Hirobe, M. *J. Am. Chem. Soc.* **1990**, *112*, 7051−7053.
(17) Rosenthal, J.; Nocera, D. G. *Acc. Chem. Res.* **2007**, *40*, 543−553.
(18) Zhu, S.; Xu, X.; Perman, J. A.; Zhang, X. P. *J. Am. Chem. Soc.* **2010**, *132*, 12796−12799.
(19) Shi, C. N.; Anson, F. C. *Inorg. Chem.* **1996**, *35*, 7928−7931.
(20) Kellett, R. M.; Spiro, T. G. *Inorg. Chem.* **1985**, *24*, 2373−2377.
(21) Fukuzumi, S.; Imahori, H.; Yamada, H.; El-Khouly, M. E.; Fujitsuka, M.; Ito, O.; Guldi, D. M. *J. Am. Chem. Soc.* **2001**, *123*, 2571−2575.
(22) Bucher, C.; Devillers, C. H.; Moutet, J.-C.; Royal, G.; Saint-Aman, E. *Coord. Chem. Rev.* **2009**, *253*, 21−36.
(23) Karlsson, A.; Parales, J. V.; Parales, R. E.; Gibson, D. T.; Eklund, H.; Ramaswamy, S. *Nature* **2003**, *299*, 1039−1042.
(24) Yoshizawa, K. *Acc. Chem. Res.* **2006**, *39*, 375−382.
(25) Sazinsky, M. H.; Lippard, S. J. *Acc. Chem. Res.* **2006**, *39*, 558−566.
(26) Solomon, E. I.; Sundaram, U. M.; Machonkin, T. E. *Chem. Rev.* **1996**, *96*, 2563−2606.
(27) Burgess, B. K. *Chem. Rev.* **1990**, *90*, 1377−1406.
(28) Chan, M. K.; Kim, J.; Rees, D. C. *Science* **1993**, *260*, 792−794.

(29) Boal, A. K.; Genereux, J. C.; Sontz, P. A.; Gralnick, J. A.; Newman, D. K.; Barton, J. K. *Proc. Natl. Acad. Sci. U. S. A.* **2009**, *106*, 15237−15242.
(30) Guigliarelli, B.; Magalon, A.; Asso, M.; Bertrand, P.; Frixon, C.; Giordano, G. r.; Blasco, F. *Biochemistry* **1996**, *35*, 4828−4836.
(31) Pershad, H. R.; Duff, J. L. C.; Heering, H. A.; Duin, E. C.; Albracht, S. P. J.; Armstrong, F. A. *Biochemistry* **1999**, *38*, 8992−8999.
(32) Beharry, Z. M.; Eby, D. M.; Coulter, E. D.; Viswanathan, R.; Neidle, E. L.; Phillips, R. S.; Kurtz, D. M. *Biochemistry* **2003**, *42*, 13625−13636.
(33) Dey, A.; Francis, E. J.; Adams, M. W. W.; Babini, E.; Takahashi, Y.; Fukuyama, K.; Hodgson, K. O.; Hedman, B.; Solomon, E. I. *Science* **2007**, *318*, 1464−1468.
(34) Solomon, E. I.; Szilagyi, R. K.; DeBeer George, S.; Basumallick, L. *Chem. Rev.* **2004**, *104*, 419−458.
(35) Kassner, R. J. *Proc. Natl. Acad. Sci. U. S. A.* **1972**, *69*, 2263−2267.
(36) Stephens, P. J.; Jollie, D. R.; Warshel, A. *Chem. Rev.* **1996**, *96*, 2491−2514.
(37) Warshel, A.; Sharma, P. K.; Kato, M.; Xiang, Y.; Liu, H.; Olsson, M. H. M. *Chem. Rev.* **2006**, *106*, 3210−3235.
(38) Samanta, S.; Sengupta, K.; Mittra, K.; Bandyopadhyay, S.; Dey, A. *Chem. Commun.* **2012**, *48*, 7631−7633.
(39) Boulatov, R.; Collman, J. P.; Shiryaeva, I. M.; Sunderland, C. J. *J. Am. Chem. Soc.* **2002**, *124*, 11923−11935.
(40) Bard, A. J.; Faulkner, L. R. *Electrochemical Methods*; Wiley: New York, 2001.
(41) Collman, J. P.; Ghosh, S.; Dey, A.; Decreau, R. A. *Proc. Natl. Acad. Sci. U. S. A.* **2009**, *106*, 22090−22095.
(42) Nourooz-Zadeh, J.; Lester, P. Ferrous ion oxidation in presence of xylenol orange for detection of lipid hydroperoxides in plasma. In *Methods in Enzymology*; Academic Press: San Diego, CA, 1999; Vol. *300*, pp 58−62.
(43) Collman, J. P.; Brauman, J. I.; Suslick, K. S. *J. Am. Chem. Soc.* **1975**, *97*, 7185−7186.
(44) D. Beer, P.; G. B. Drew, M.; Jagessar, R. *J. Chem. Soc., Dalton Trans.* **1997**, 881−886.
(45) Mandon, D.; Ott-Woelfel, F.; Fischer, J.; Weiss, R.; Bill, E.; Trautwein, A. X. *Inorg. Chem.* **1990**, *29*, 2442−2447.
(46) Ricard, D.; L'Her, M.; Richard, P.; Boitrel, B. *Chem.—Eur. J.* **2001**, *7*, 3291−3297.
(47) K. Burrell, A.; M. Campbell, W.; B. Jameson, G.; L. Officer, D.; D. W. Boyd, P.; Zhao, Z.; A. Cocks, P.; C. Gordon, K. *Chem. Commun.* **1999**, 637−638.
(48) Nemykin, V. N.; Barrett, C. D.; Hadt, R. G.; Subbotin, R. I.; Maximov, A. Y.; Polshin, E. V.; Koposov, A. Y. *Dalton Trans.* **2007**, 3378−3389.
(49) Mu, X. H.; Schultz, F. A. *Inorg. Chem.* **1990**, *29*, 2877−2879.
(50) Collman, J. P.; Gagne, R. R.; Reed, C.; Halbert, T. R.; Lang, G.; Robinson, W. T. *J. Am. Chem. Soc.* **1975**, *97*, 1427−1439.
(51) Ghiladi, R. A.; Karlin, K. D. *Inorg. Chem.* **2002**, *41*, 2400−2407.
(52) Thompson, D. W.; Kretzer, R. M.; Lebeau, E. L.; Scaltrito, D. V.; Ghiladi, R. A.; Lam, K.-C.; Rheingold, A. L.; Karlin, K. D.; Meyer, G. J. *Inorg. Chem.* **2003**, *42*, 5211−5218.
(53) Burke, J. M.; Kincaid, J. R.; Peters, S.; Gagne, R. R.; Collman, J. P.; Spiro, T. G. *J. Am. Chem. Soc.* **1978**, *100*, 6083−6088.
(54) Note that the ν_4 and ν_2 values for a four coordinate and six coordinate Fe(II) porphyrin species are at 1370 cm^{-1} and 1608 cm^{-1} and 1354 cm^{-1} and 1557 cm^{-1}, respectively.
(55) Ghiladi, R. A.; Kretzer, R. M.; Guzei, I.; Rheingold, A. L.; Neuhold, Y.-M.; Hatwell, K. R.; Zuberbãhler, A. D.; Karlin, K. D. *Inorg. Chem.* **2001**, *40*, 5754−5767.
(56) Latos-Grazynski, L.; Cheng, R. J.; La Mar, G. N.; Balch, A. L. *J. Am. Chem. Soc.* **1982**, *104*, 5992−6000.
(57) Jameson, G. B.; Molinaro, F. S.; Ibers, J. A.; Collman, J. P.; Brauman, J. I.; Rose, E.; Suslick, K. S. *J. Am. Chem. Soc.* **1980**, *102*, 3224−3237.
(58) Collman, J. P.; Gagne, R. R.; Halbert, T. R.; Marchon, J. C.; Reed, C. A. *J. Am. Chem. Soc.* **1973**, *95*, 7868−7870.
(59) Phillippi, M. A.; Shimomura, E. T.; Goff, H. M. *Inorg. Chem.* **1981**, *20*, 1322−1325.
(60) Fleischer, E. B.; Palmer, J. M.; Srivastava, T. S.; Chatterjee, A. *J. Am. Chem. Soc.* **1971**, *93*, 3162−3167.
(61) Chang, P.; Wilke, C. R. *J. Phys. Chem.* **1955**, *59*, 592−596.
(62) McCrory, C. C. L.; Ottenwaelder, X.; Stack, T. D. P.; Chidsey, C. E. D. *J. Phys. Chem. A* **2007**, *111*, 12641−12650.
(63) Shi, C.; Anson, F. C. *Inorg. Chem.* **1998**, *37*, 1037−1043.
(64) Devaraj, N. K.; Decreau, R. A.; Ebina, W.; Collman, J. P.; Chidsey, C. E. D. *J. Phys. Chem. B* **2006**, *110*, 15955−15962.
(65) Shi, C.; Anson, F. C. *Inorg. Chem.* **1995**, *34*, 4554−4561.
(66) Naik, A. D.; Dîrtu, M. M.; Léonard, A.; Tinant, B.; Marchand-Brynaert, J.; Su, B.-L.; Garcia, Y. *Cryst. Growth Des.* **2010**, *10*, 1798−1807.
(67) Mittra, K.; Chatterjee, S.; Samanta, S.; Sengupta, K.; Bhattacharjee, H.; Dey, A. *Chem. Commun.* **2012**, *48*, 10535.
(68) Vogel, K. M.; Kozlowski, P. M.; Zgierski, M. Z.; Spiro, T. G. *J. Am. Chem. Soc.* **1999**, *121*, 9915−9921.
(69) Matson, B. D.; Carver, C. T.; Von Ruden, A. L.; Yang, J.; Raugei, S.; Mayer, J. *Chem. Commun.* **2012**, *48*, 11100−11102.
(70) MacBeth, C. E.; Golombek, A. P.; Young, V. G., Jr; Yang, C.; Kuczera, K.; Hendrich, M. P.; Borovik, A. S. *Science* **2000**, *289*, 938−941.
(71) Ferguson-Miller, S.; Babcock, G. T. *Chem. Rev.* **1996**, *96*, 2889−2908.
(72) Burgess, B. K.; Lowe, D. J. *Chem. Rev.* **1996**, *96*, 2983−3012.